Proton /oxygen ion conductivity ratio of Nd containing $La_{10}W_2O_{21}/\gamma$-$La_6W_2O_{15}$ tungstates

A.V. Shlyakhtina [a,*], *E.D. Baldin* [a], *G.A. Vorobieva* [a], *I.V. Kolbanev* [a],
D.N. Stolbov [b], *A.V. Kasyanova* [c,d], *N.V. Lyskov* [e,f]

[a] *N.N. Semenov Federal Research Center for Chemical Physics, Russian Academy of Sciences, Moscow, Russia*
[b] *Department of Chemistry, Lomonosov Moscow State University, Leninskie Gory 1-3, Moscow, Russia*
[c] *Institute of High Temperature Electrochemistry, Ural Branch, RAS, Ekaterinburg, Russia*
[d] *Ural Federal University Named After the First President of Russia B.N. Yeltsin, Ekaterinburg, Russia*
[e] *Federal Research Center of Problems of Chemical Physics and Medical Chemistry RAS, Moscow Region, Chernogolovka, Russia*
[f] *National Research University "Higher School of Economics", Moscow, Russia*

HIGHLIGHTS

- Proton conductivity of Nd containing γ-$La_6W_2O_{15}$-based composites is studied.
- Pseudorhombohedral $La_{14-x}Nd_xW_4O_{33}$ (x = 12, 14) are new oxygen-ion conductors.
- Reversible phase transition near 910 °C, suppressed by Nd introduction into the composite.
- Synthesis at T ≥ 1500 °C leads to the WO_3 evaporation from La/Nd mixed tungstates.
- $La_{10}W_2O_{21}$-based composite approaches conductivity of $La_{6-x}WO_{12-\delta}$ proton conductors.

GRAPHICAL ABSTRACT
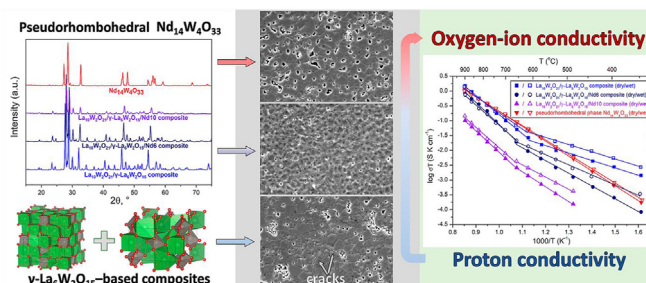
ARTICLE INFO

ABSTRACT

The search for new materials with pronounced proton or oxygen-ion conductivities is of great importance for the development of solid state ionic and electrochemistry fields. Here, we studied the structure, phase transitions, and ionic (oxygen-ion and proton) conductivity of the pure and Nd containing γ-$La_6W_2O_{15}$-based composites and pseudorhombohedral $La_{14-x}Nd_xW_4O_{33}$ (x = 12, 14) solid solutions. The proton conductor $La_{14}W_4O_{33}$ (5×10^{-5} S/cm at 600 °C) was found to be a two-phase material consisting of an anion-deficient $La_{10}W_2O_{21}$ fluorite-related phase and the γ-$La_6W_2O_{15}$ orthorhombic phase. The phase content of the pure $La_{10}W_2O_{21}$ cubic phase was ~18 wt% for the γ-$La_6W_2O_{15}$-based composite. A high degree of Nd content in γ-$La_6W_2O_{15}$-based composite leads to formation of solid solutions based on a pseudorhombohedral phase in $La_{14-x}Nd_xW_4O_{33}$ with x = 12 and 14. The Nd

---

* *Corresponding author.* N.N. Semenov Federal Research Center for Chemical Physics, RAS, Moscow 119991, Russia
E-mail addresses: annashl@inbox.ru, annash@chph.ras.ru (A.V. Shlyakhtina).

Two phase composites
Proton conductivity
Oxygen-ion conductivity

-containing γ-La$_6$W$_2$O$_{15}$-based composites exhibited proton conductivity, which gradually decreased with increasing Nd content, whereas La$_{14-x}$Nd$_x$W$_4$O$_{33}$ (x = 12, 14) pseudo-rhombohedral solid solutions were identified as oxygen-ion conductors. Nd$_{14}$W$_4$O$_{33}$ has the oxygen -ion conductivity of ~4 × 10^{-4} S/cm at 700 °C (1.0 × 10^{-3} S/cm at 900 °C). In contrast to the γ-La$_6$W$_2$O$_{15}$ phase, the γ-La$_6$W$_2$O$_{15}$-based composite undergoes only a single reversible phase transition at around 910 °C, which can, however, initiate cracks in ceramics. According to DSC and SEM data, the phase transition near 910 °C can be suppressed by introducing Nd into the γ-La$_6$W$_2$O$_{15}$-based composites. The cracking process is enhanced by evaporation of tungsten oxide at T ≥ 1450 °C.

Introduction

Complex lanthanum-containing oxides with pronounced proton transfer are of great interest from both fundamental and applied points of view [1–5]. Interest in the La$_2$O$_3$ − MoO$_3$ and La$_2$O$_3$ − WO$_3$ systems is aroused by the fact that they contain compounds and solid solutions with high oxygen ion and proton conductivity. They include La$_2$Mo$_2$O$_9$ [6,7], La$_{6-x}$MoO$_{12-\delta}$ [6–8], La$_2$W$_2$O$_9$ (high-temperature phase) [9], La$_{10}$W$_2$O$_{21}$ [10], and La$_{6-x}$WO$_{12-\delta}$ (x = 0.3−0.7) [11–17]. The highest proton conductivity so far has been found in 20% rhenium substituted La$_{6-x}$WO$_{12-\delta}$ (x = 0.5) lanthanum tungstate: ~4 × 10^{-3} S/cm at 800 °C in wet H$_2$ [18].

La$_{6-x}$WO$_{12-\delta}$ (x = 0.6) solid solutions [15,19] have the highest conductivity among the mentioned compounds, which is potentially suitable for their utilization as proton-conducting electrolytes for solid oxide fuel cells. When doped with molybdenum in the tungsten sublattice, the material can be used to fabricate dense membranes for pure hydrogen generation [15,18,19].

However, a later study of La$_{27}$(W, Mo)$_5$O$_{55.5-\delta}$ − La$_{0.87}$Sr$_{0.13}$CrO$_{3-\delta}$ composite membranes exposed to a gas flow containing 45% hydrogen and 2.5% water at 900 °C for 1500 h [20] revealed lanthanum oxide segregation, which led to a drop in the ionic conductivity of the membrane. In addition, the lanthanum tungstate was found to undergo partial degradation and reduction to metallic tungsten [20]. Thus, despite the high proton conductivity of the La$_{6-x}$WO$_{12-\delta}$ (x = 0.3−0.7) fluorite-related solid solutions, these materials turned out to be insufficiently stable under reducing conditions [20].

As shown by Pestereva et al. [21,22] using the Tubandt method, not only oxygen transport but also [WO$_4$]$^{2-}$ ion transport is possible in Ln_2(WO$_4$)$_3$ (Ln_2O$_3$:3WO$_3$ (1:3)) — rare-earth tungstates considerably richer in tungsten oxide. The contribution of the [WO$_4$]$^{2-}$ ions to their conductivity is rather small: the corresponding transference number does not exceed 5%. In addition, it was pointed out that this type of ion transport led to changes in the composition of the material. In a number of cases, X-ray powder diffraction results indicated formation of new phases near electrodes. For example, La$_6$WO$_{12}$ and La$_{10}$W$_{22}$O$_{81}$ impurities were detected on cathodic and anodic La$_2$(WO$_4$)$_3$ surfaces that were in contact with the electrodes. In the case of Lu$_2$(WO$_4$)$_3$, Lu$_6$WO$_{12}$ was formed in a tungsten-deficient region and WO$_3$ appeared on the surface of a tungsten-enriched region.

Partial or complete substitution of La to Nd in La$_{6-x}$WO$_{12-\delta}$ solid solutions has been a subject of several studies [23–26]. Such Nd-doping leads to a systematic decrease in the proton conductivity of La$_{6-x}$WO$_{12-\delta}$. This behavior can be explained in terms of differences in the hydration degree and defect density, both of which affect proton conductivity [27]. At the same time, hydrogen flux through tungstate membranes with a large lanthanum-to-neodymium ratio ((La$_{5/6}$Nd$_{1/6}$)$_{5.5}$WO$_{12-\delta}$) and a small one ((Nd$_{5/6}$La$_{1/6}$)$_{5.5}$WO$_{12-\delta}$) was the same, despite the higher total proton conductivity of La-rich membranes [25].

Ln_{14}W$_4$O$_{33}$ compounds exist in the Ln_2O$_3$−WO$_3$ (Ln = Nd−Lu, Y) systems [28–32] but not in the Ln_2O$_3$−WO$_3$ (Ln = La, Ce) systems [33,34]. Formation of Nd$_{14}$W$_4$O$_{33}$ (7Nd$_2$O$_3$: 4WO$_3$ (7:4)) in the Nd$_2$O$_3$−WO$_3$ system was confirmed by McCarthy et al. [28], whereas the La$_2$O$_3$−WO$_3$ system was reported to contain La$_6$W$_2$O$_{15}$ (3La$_2$O$_3$:2WO$_3$ (3:2)) instead [25]. According to an early phase diagram [35], in the Nd$_2$O$_3$−WO$_3$ system only one compound is formed (Nd$_4$WO$_9$) without appearance of Nd$_{14}$W$_4$O$_{33}$. Later, La$_6$W$_2$O$_{15}$ phase was studied in details by Chambrier [36] and Chambrier et al. [37]. The high-temperature α-La$_6$W$_2$O$_{15}$ phase crystallizes in the non-centrosymmetric orthorhombic space group (No.20) of C2221, with Z = 2, a = 12.6250 (2) Å, b = 9.1875 (1) Å, c = 5.9688 (1) Å. There are also two low temperature phases, β-La$_6$W$_2$O$_{15}$ and γ-La$_6$W$_2$O$_{15}$, which are similar in structure. The structure of γ-La$_6$W$_2$O$_{15}$ was reported much earlier by Yoshimura [38]. The temperatures of the $\gamma \to \beta$ and $\beta \to \alpha$ reversible polymorphic transformations were close to ~615 and ~945 °C, respectively [37]. Note that the La$_6$W$_2$O$_{15}$ compound, like La$_{10}$W$_2$O$_{21}$, lies in the La$_2$O$_3$-rich region that contains well-known La$_{6-x}$WO$_{12-\delta}$ (x = 0.3−0.7) proton conductors. Ivanova et al. [39] studied the effect of La$_6$W$_2$O$_{15}$ as impurity phase on the properties and integrity of La$_{6-x}$WO$_{12-\delta}$-based membranes. La$_6$W$_2$O$_{15}$ is a rather stable phase, which is often formed as an impurity during synthesis of La$_{6-x}$WO$_{12-\delta}$ proton conductors. Its proton conductivity is lower (by one to two orders of magnitude) than that of La$_{6-x}$WO$_{12-\delta}$, and it has a more pronounced tendency to hydrate [39]. The structure and oxygen ion conductivity of La$_{10}$W$_2$O$_{21}$ were studied in detail by

Chambrier et al. [12], while this compound was not reported to have proton conductivity. The crystal structure of $La_{10}W_2O_{21}$ can be described by a $2 \times 2 \times 2$ anion-deficient fluorite-related superstructure cubic cell, with space group of F $\overline{4}$ 3 m, Z = 4, and a = 11.17932 (6) Å, similar to $Y_7ReO_{14-\delta}$. Many compounds in the $La_2O_3-MO_3$ (M = Mo, W) systems are known to have large, complex unit cells [6–10,13–15].

The structure type of $Ln_{14}W_4O_{33}$ compounds of light and intermediate lanthanides remains the subject of controversy. According to McCarthy et al. [28], in the case of the intermediate lanthanide compounds, $Ln_{14}W_4O_{33}$ (Ln = Ho, Y), the three strongest lines of their rhombohedral structure (214, 413, and 422) have the form of doublets and cannot be indexed in a simple rhombohedral cell. The structure of $Ln_{14}W_4O_{33}$ (Ln = Nd−Dy) with most lines split into doublets, is even more distorted. Because of this, the structure of the $Ln_{14}W_4O_{33}$ (Ln = Nd−Ho, Y) compounds is thought to be pseudo-rhombohedral, and their lattice parameters were determined using only four unsplit lines [28,31,40].

In this paper, we report the structure, oxygen ion and proton conductivity of γ-$La_6W_2O_{15}$-based and $La_{10}W_2O_{21}$-based composites, respectively. We present the first oxygen ion and proton conductivity study for Nd containing γ-$La_6W_2O_{15}$-based composites and pseudorhombohedral $La_{14-x}Nd_xW_4O_{33}$ (x = 12, 14) solid solutions. The influence of neodymium introduction into γ-$La_6W_2O_{15}$-based composites on the reversible phase transition and strengthening of proton-conducting ceramics will be investigated. A $La_{10}W_2O_{21}$-based composite (~80 wt% pure $La_{10}W_2O_{21}$) with high proton conductivity approaching that of $La_{6-x}WO_{12-\delta}$ (x = 0.6) fluorite-like proton conductor will be found.

Experimental part

The nominal compositions $La_{14-x}Nd_xW_4O_{33}$ (x = 0, 2, 4, 6, 8, 10, 12, 14) and $La_{10}W_2O_{21}$ were synthesized by reacting appropriate oxide mixtures ($La_2O_3 + Nd_2O_3 + WO_3$) after mechanical activation in the Aronov ball mill [41,42]. The parameters of Aronov ball mill were reported in Ref. [43]. Starting powders of La_2O_3 and Nd_2O_3 were annealed at 1000 °C for 2 h and then placed in a desiccator after cooling to 850 °C. After milling, mixtures were pressed at 650 MPa and then fired at 1300 °C−1600 °C for 2−8 h in air. Additionally, a fluorite-like $La_{6-x}WO_{12-\delta}$ (x = 0.7) proton conductor with a high La_2O_3 content was synthesized at a temperature of 1640 °C. It was studied to refine its local structure by Raman spectroscopy and to compare it with that of $La_{14}W_4O_{33}$ material. The density of sintered samples was determined by measuring their weight and dimensions. Table S1 shows characteristics of studied samples (nominal compositions, abbreviations, synthesis conditions, density, structure type and colour).

X-ray diffraction (XRD) patterns for the powder samples were collected at room temperature on a DRON-3M automatic diffractometer (Cu K_α radiation, λ = 1.5418 Å, Bragg-reflection geometry, 35 kV, 28 mA) in the 2θ range of 10°−75° (scan step of 0.1° τ = 3 s). Additionally, for some ceramics XRD patterns were also collected at room temperature with a Rigaku Smartlab SE X-ray diffractometer (Cu K_α radiation, λ = 1.5418 Å, Bragg-reflection geometry, 40 kV, 50 mA) in

continuous mode. The 2θ range was 10°−70°, scan step 0.01°, scan rate 5°/min. Rietveld refinement was carried out using the SmartLab Studio II software. Relative weight fractions in biphasic samples were determined automatically by the software after fitting according to the formula presented in Hill & Howard (1987) [44].

The microstructure of ceramic samples was examined by scanning electron microscopy (SEM) on a JEOL JSM-6390LA, which was also used to perform energy dispersive X-ray microanalysis (EDX) and to obtain selected-element X-ray maps. Using the SEM method, we analysed the cation ratio on the polished and thermal etched or fresh fracture surfaces.

Thermogravimetric analysis was performed by using the NETZSCH STA 449C system (50−1000 °C, a heating rate of 10 °C/min, Al_2O_3 plate) in air for nominal $La_{14-x}Nd_xW_4O_{33}$ (x = 0, 2, 4, 6, 8, 10, 12, 14) ceramics. We aimed to study the dynamics of phase transitions typical for γ-$La_6W_2O_{15}$. We performed TG scans from 50 to 1000 °C in an oxygen atmosphere on heating − cooling mode.

For electrical measurements, the disk-shaped polycrystalline samples (diameter ~ 9 mm and thickness 2−3 mm) were prepared. Contacts to the sample surfaces were made by firing ChemPur C3605 paste, containing colloidal platinum, at 950−1000 °C. The conductivity of composites and solutions was studied by impedance spectroscopy in dry and wet air. The technique for measuring conductivity in dry and wet air on cooling was presented in Ref. [45].

In addition, the total conductivity of $Nd_{14}W_4O_{33}$ was evaluated by the four-probe DC method. The measurements were performed on a Zirconia-M microprocessor system at temperatures from 700 to 900 °C in dry and in wet oxidizing and reducing atmospheres (air, N_2, H_2). Wet atmospheres (P_{H2O} = 0.02 atm) were generated by bubbling gases through water at 18 °C. In addition, the total conductivity of $Nd_{14}W_4O_{33}$ was measured as a function of oxygen partial pressure in the range of 700−900 °C.

Results and discussion

The structure of materials studied by X-ray diffraction (XRD) and Raman spectroscopy

Structure of $7Ln_2O_3$:$4WO_3$ (Ln = La, Nd) materials by XRD study
Fig. S2a shows powder XRD patterns of $7La_2O_3$:$4WO_3$ ceramics sintered at 1300, 1450, and 1600 °C. It is worth noting that, after high-temperature annealing at 1600 °C, signs of melting were observed on the surface of ceramics (Fig. S2b). The melting point of $7La_2O_3$:$4WO_3$ composition is lower than that of $La_{6-x}WO_{12-\delta}$ solid solutions (based on La_6WO_{12} ($3La_2O_3$:WO_3)), which melt at ~1900 °C [33]. XRD patterns of the bulk and surface of $7La_2O_3$:$4WO_3$ pellets prepared at 1600 °C (Fig. S2b, curves 1 and 2) differ markedly. The presence of impurity phases on the surface is obvious (Fig. S2b, curve 1). In view of this, $7La_2O_3$:$4WO_3$ ceramics were prepared by firing at 1450 °C for 4 h. As a result, we obtained identical XRD patterns of the surface of the pellet and powder prepared from it. According to XRD data (Fig. 1, Table 1), $7La_2O_3$:$4WO_3$ is two-phase material consisting of the mixture of fluorite-related $La_{10}W_2O_{21}$
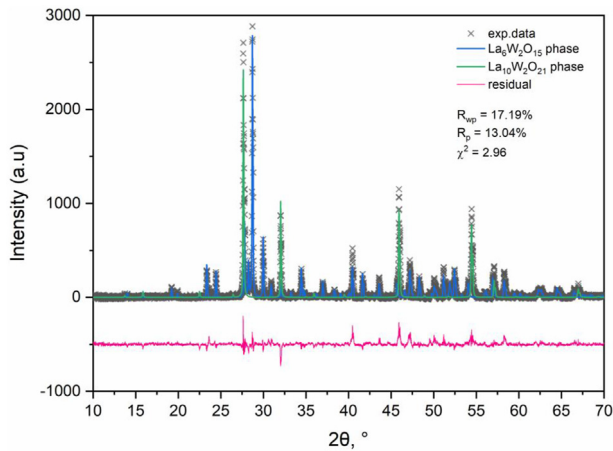
Fig. 1 – Rietveld refinement results for the powder prepared by grinding the ceramic with the nominal composition $7La_2O_3:4WO_3$ prepared at 1450 °C (4 h). The material consists of two phases: fluorite-related $La_{10}W_2O_{21}$ ($5La_2O_3:2WO_3$) (ICDD PDF 30–687) and γ-$La_6W_2O_{15}$ ($3La_2O_3:2WO_3$) (ICDD PDF 31–374).

phase ($5La_2O_3:2WO_3$) (ICDD PDF 30–687) (~18 wt%) and γ-$La_6W_2O_{15}$ ($3La_2O_3:2WO_3$) (ICDD PDF 31–374) (~82 wt%), in perfect agreement with phase diagram data [33]. Actually, we have synthesized γ-$La_6W_2O_{15}$-based composite.

It is worth noting here a negative feature of the $La_2O_3-WO_3$ system, in which most of the compounds have a very narrow

homogeneity range, within 3 mol %, if any. This feature is certainly a serious obstacle to cation doping of the compounds of this system and preparation of various highly conductive materials [15].

$Nd_{14}W_4O_{33}$ was synthesized at 1200, 1400, 1450, 1500, and 1600 °C using different isothermal holding times (3, 4, and 8 h). High-temperature annealing at 1600 °C was found to cause partial surface melting of ceramics, like in the case of lanthanum tungstate γ-$La_6W_2O_{15}$-based composite. Fig. S3 shows XRD patterns of the high-conductive (curve 1) and low-conductive (curve 2) $Nd_{14}W_4O_{33}$ ceramics prepared at 1400 and 1500 °C, respectively. The conductivity of these phases will be discussed further. No impurity phases were detected. The pseudorhombohedral cell parameters of $Nd_{14}W_4O_{33}$ synthesized at the optimal temperature (1450 °C, 4 h) were determined to be $a = 10.049$ (4) Å and $c = 9.775$ (8) Å as evaluated from ten lines, of which six were split into doublets, or $a = 10.050$ (3) Å and $c = 9.790$ (8) Å from the four unsplit lines, in good agreement with the literature data [28], especially in the former case.

Structure of Nd-containing lanthanum tungstates with the nominal composition $La_{14-x}Nd_xW_4O_{33}$ ($x = 0, 2, 4, 6, 8, 10, 12$)
Most Nd-containing materials are a mixture of $La_{10}W_2O_{21}$ ($5La_2O_3:2WO_3$) (ICDD PDF 30–687) and γ-$La_6W_2O_{15}$ ($3La_2O_3:2WO_3$) (ICDD PDF 31–374) (Fig. 2a, curves 1–6). The Nd-containing composite materials contain ~15–19 wt% of the $La_{10}W_2O_{21}$ phase and ~81–85 wt% of the γ-$La_6W_2O_{15}$ (Table 1). Only at a high Nd content, for $La_{14-x}Nd_xW_4O_{33}$

Table 1 – Unit cell parameters of γ-$La_6W_2O_{15}$-based composite, Nd - containing γ-$La_6W_2O_{15}$-based composites (γ-$La_6W_2O_{15}$/$La_{10}W_2O_{21}$/Ndx ($x = 0, 2, 4, 6, 8, 10$)), and $La_{10}W_2O_{21}$-based composite synthesized at 1500 °C.

x	Phase γ-$La_6W_2O_{15}$ - (3:2) content, wt%	Cell parameters of γ-$La_6W_2O_{15}$ (3:2) phase, Å	Phase $La_{10}W_2O_{21}$ -($5La_2O_3:2WO_3$) - (5:2) content,wt%	Cell parameter of $La_{10}W_2O_{21}$ (5:2) phase, Å	Rwp, %	Rp, %	χ^2
γ-$La_6W_2O_{15}$-based composite materials							
0[a]	81.7 (2)	a, 12.6235 (7) b, 8.9097 (5) c, 5.9569 (3)	18.3 (2)	11.1657 (6)	17.19	13.04	2.96
2	81.88 (14)	a, 12.5878 (9) b, 8.8922 (6) c, 5.9484 (4)	18.12 (14)	11.1084 (7)	16.65	11.83	3.44
4	84.44 (16)	a, 12.5575 (6) b, 8.8621 (4) c, 5.9394 (3)	15.56 (16)	11.0702 (4)	13.80	9.76	4.88
6	84.65 (17)	a, 12.5238 (8) b, Å 8.8361 (5) c, Å 5.9210 (3)	15.35 (17)	11.0296 (6)	13.01	9.37	4.10
8	83.18 (17)	a, 12.4837 (8) b, 8.8133 (6) c, 5.9072 (4)	16.82 (17)	10.9990 (5)	13.56	9.52	3.87
10	81.1 (2)	a, 12.4427 (10) b, 8.7853 (6) c, 5.8943 (4)	18.9 (2)	10.9684 (5)	12.70	9.22	3.48
$La_{10}W_2O_{21}$-based composite material							
0	19.4 (8)	a, 12.490 (2) b, 9.0134 (2) c, 5.8931 (7)	80.6 (8)	11.1685 (5)	11.85	7.6	3.55

[a] γ-$La_6W_2O_{15}$-based composite was synthesized at 1450 °C, 4 h.

(a)

(b)

(c)
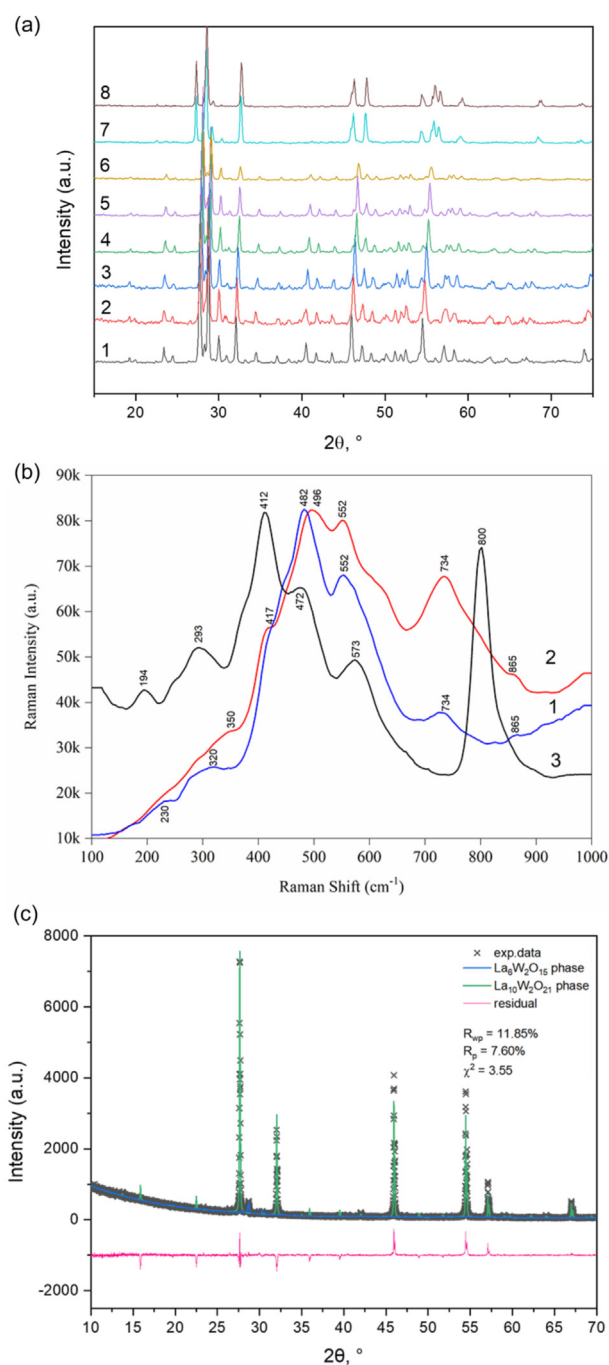
Fig. 2 – a: XRD patterns of the γ-La$_6$W$_2$O$_{15}$–based composite materials: ((1) La$_{10}$W$_2$O$_{21}$/γ-La$_6$W$_2$O$_{15}$, (2) La$_{10}$W$_2$O$_{21}$/γ-La$_6$W$_2$O$_{15}$/Nd2, (3) La$_{10}$W$_2$O$_{21}$/γ-La$_6$W$_2$O$_{15}$/Nd4, (4) La$_{10}$W$_2$O$_{21}$/γ-La$_6$W$_2$O$_{15}$/Nd6, (5) La$_{10}$W$_2$O$_{21}$/γ-La$_6$W$_2$O$_{15}$/Nd8, (6) La$_{10}$W$_2$O$_{21}$/γ-La$_6$W$_2$O$_{15}$/Nd10), and pseudorhombohedral solid solutions (7) La$_2$Nd$_{12}$W$_4$O$_{33}$, (8) Nd$_{14}$W$_4$O$_{33}$ synthesized at 1450–1500 °C, illustrating change in structure type in response to Nd incorporation in the γ-La$_6$W$_2$O$_{15}$ based composite. b: Raman spectra of the γ-La$_6$W$_2$O$_{15}$–based composite materials: (1) La$_{10}$W$_2$O$_{21}$/γ-La$_6$W$_2$O$_{15}$, (2) La$_{10}$W$_2$O$_{21}$/γ-La$_6$W$_2$O$_{15}$/Nd2, and (3) highly conductive fluorite-related proton conductor La$_{5.3}$WO$_{10.95}$. c: Rietveld refinement results for La$_{10}$W$_2$O$_{21}$–based composite material prepared at 1500 °C (4 h). The material

($x = 12$), we observed formation of Nd$_{14}$W$_4$O$_{33}$-based pseudo-rhombohedral solid solution (Fig. 2a, curves 7, 8). Fig. 2a (curves 6, 7) clearly shows the structural type change.

Table 1 shows the Rietveld refinement data for composite materials, from which it follows that the cell parameters decrease with increasing Nd content for both La$_{10}$W$_2$O$_{21}$ (5La$_2$O$_3$:2WO$_3$) and γ-La$_6$W$_2$O$_{15}$ (3La$_2$O$_3$:2WO$_3$) systems. The most probable scenario is doping of both phases with neodymium, which will be confirmed below by SEM.

XRD patterns of La$_{10}$W$_2$O$_{21}$/γ-La$_6$W$_2$O$_{15}$ and La$_{10}$W$_2$O$_{21}$/γ-La$_6$W$_2$O$_{15}$/Nd2 composite materials show that they have similar crystal structure (Fig. 2a, curves 1, 2). Raman spectroscopy results (Fig. 2b, spectra 1, 2) demonstrate that La$_{10}$W$_2$O$_{21}$/γ-La$_6$W$_2$O$_{15}$ and La$_{10}$W$_2$O$_{21}$/γ-La$_6$W$_2$O$_{15}$/Nd2 composite materials have the same short-range order structure. For comparison, the Raman spectrum of the well-known fluorite-related proton conductor La$_{6-x}$WO$_{12-\delta}$ ($x = 0.7$) (La$_{5.3}$WO$_{10.95}$) is also shown in Fig. 2b (spectrum 3). Clearly, the composite materials, La$_{10}$W$_2$O$_{21}$/γ-La$_6$W$_2$O$_{15}$ and La$_{10}$W$_2$O$_{21}$/γ-La$_6$W$_2$O$_{15}$/Nd2, differ in the short-range order structure from the highly conductive fluorite-related solid solution La$_{6-x}$WO$_{12-\delta}$ ($x = 0.7$).

Fig. 2c and Table 1 demonstrate the Rietveld refinement data for material with nominal composition 5La$_2$O$_3$:2WO$_3$ (T$_{syn.}$ = 1500 °C, 4 h). It is clear that in this case the composite material is also obtained. The phase ratio La$_{10}$W$_2$O$_{21}$/γ-La$_6$W$_2$O$_{15}$ is reversed in this case compared to the 7La$_2$O$_3$:4WO$_3$ composition (Table 1). Two-phase material of nominal composition 5La$_2$O$_3$:2WO$_3$ includes ~80.6 wt% of pure La$_{10}$W$_2$O$_{21}$ and ~19.4 wt% of γ-La$_6$W$_2$O$_{15}$. Actually, this is a La$_{10}$W$_2$O$_{21}$-based composite material.

Proton and oxygen-ion conductivity of Nd containing γ-La$_6$W$_2$O$_{15}$-based and La$_{10}$W$_2$O$_{21}$-based composites

Further in the text, we will use the formula La$_{10}$W$_2$O$_{21}$/γ-La$_6$W$_2$O$_{15}$/Ndx ($x = 0, 2, 4, 6, 8, 10$) to designate two-phase materials. Table S1 presents nominal compositions and formulas to designate composites for clarity.

Fig. 3a illustrates variation of the proton/oxygen ion conductivity ratio of Nd -containing lanthanum tungstates. Impedance spectra of some composites La$_{10}$W$_2$O$_{21}$/γ-La$_6$W$_2$O$_{15}$/Ndx ($x = 0, 2$) and Nd$_{14}$W$_4$O$_{33}$ are presented in the Supplementary material section (Fig. S4a-c).

γ-La$_6$W$_2$O$_{15}$-based composite has the highest proton conductivity: 6×10^{-5} S/cm at 600 °C in wet air. This is an order of magnitude higher than the proton conductivity of pure γ-La$_6$W$_2$O$_{15}$ synthesized by Ivanova et al. [39]. The proton conductivity of the La$_{10}$W$_2$O$_{21}$/γ-La$_6$W$_2$O$_{15}$/Nd2 composites with low neodymium content is lower by a factor of 2 (Fig. 3b, curve 2). As the degree of substitution increases in La$_{10}$W$_2$O$_{21}$/γ-La$_6$W$_2$O$_{15}$/Nd4 and La$_{10}$W$_2$O$_{21}$/γ-La$_6$W$_2$O$_{15}$/Nd6 composite materials, proton conductivity further decreases, to 1×10^{-5} S/cm at 600 °C (Fig. 3a, curve 2; Fig. 3b, curve 3). The proton

consists of two phases: fluorite-related La$_{10}$W$_2$O$_{21}$ (5La$_2$O$_3$:2WO$_3$) (ICDD PDF 30–687) and γ-La$_6$W$_2$O$_{15}$ (3La$_2$O$_3$:2WO$_3$) (ICDD PDF 31–374).
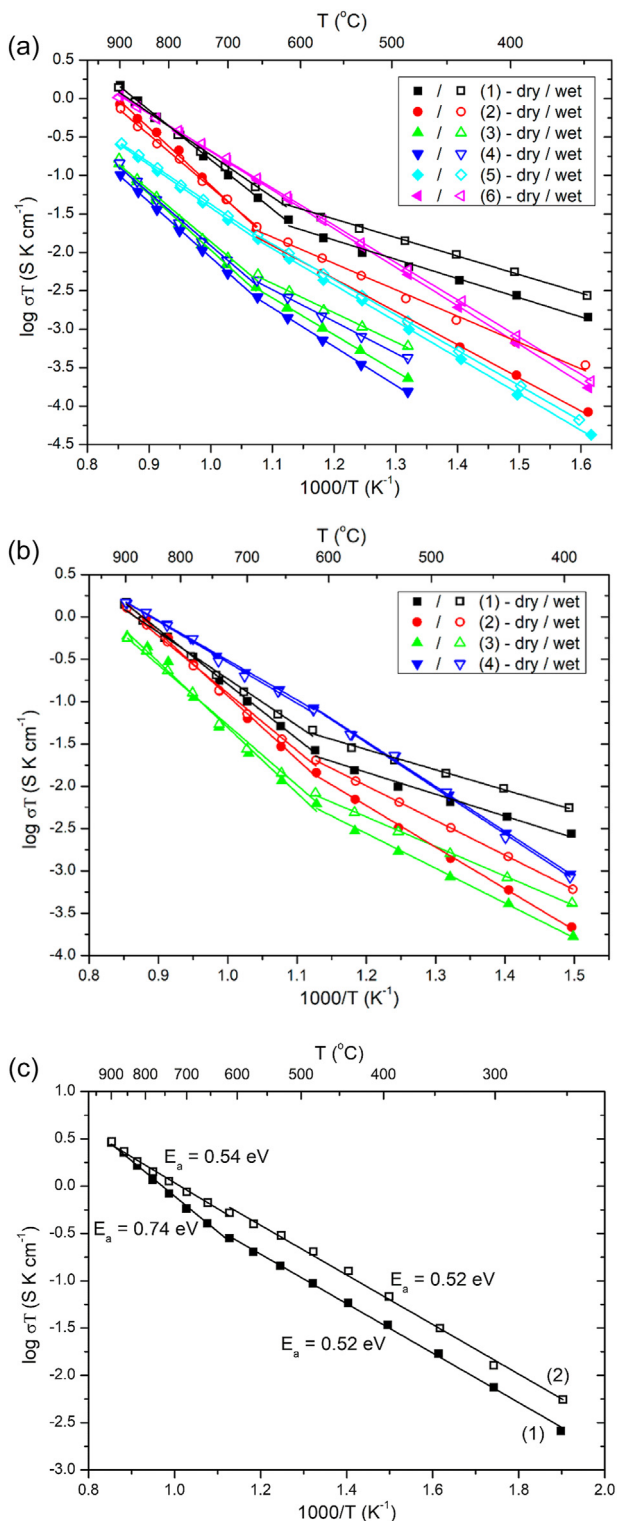
Fig. 3 — a: Arrhenius plots of conductivity in dry (filled data points) and wet (open data points) air for γ-$La_6W_2O_{15}$—based composites and pseudorhombohedral solid solutions, synthesized between 1450 and 1500 °C: (1) $La_{10}W_2O_{21}$/γ-$La_6W_2O_{15}$ composite (1450°C); (2) $La_{10}W_2O_{21}$/γ-$La_6W_2O_{15}$/Nd6 composite (1500°C); (3) $La_{10}W_2O_{21}$/γ-$La_6W_2O_{15}$/Nd8 composite (1500°C); (4) $La_{10}W_2O_{21}$/γ-$La_6W_2O_{15}$/Nd10 composite (1500°C); (5) $La_2Nd_{12}W_4O_{33}$ pseudorhombohedral solid solution (1500°C); (6) $Nd_{14}W_4O_{33}$ (1500°C). b: Arrhenius plots of conductivity in dry (filled data points) and wet (open data points) air for γ-$La_6W_2O_{15}$—based composites with low neodymium content ($x = 0$, 2, 4) and pseudorhombohedral $Nd_{14}W_4O_{33}$ synthesized between 1400 and 1450 °C: (1) $La_{10}W_2O_{21}$/γ-$La_6W_2O_{15}$ composite (1450°C); (2) $La_{10}W_2O_{21}$/γ-$La_6W_2O_{15}$/Nd2 composite (1400°C); (3) $La_{10}W_2O_{21}$/γ-$La_6W_2O_{15}$/Nd4 composite (1400°C); (4) $Nd_{14}W_4O_{33}$ (1450°C). c: Arrhenius plots of conductivity in dry (1) and wet (2) air for the $La_{10}W_2O_{21}$-based composite.

conductivity of $La_{10}W_2O_{21}$/γ-$La_6W_2O_{15}$/Nd8 and $La_{10}W_2O_{21}$/γ-$La_6W_2O_{15}$/Nd10 composite materials persists up to 650 °C, but is noticeably lower: ~4×10^{-6} S/cm at 600 °C (Fig. 3a, curves 3, 4). The break in the 600—750 °C temperature range, typical of proton conductors [8,9,46], is small in the case of $La_2Nd_{12}W_4O_{33}$ pseudorhombohedral solid solution (Fig. 3a, curve 5) and almost disappears in the case of $Nd_{14}W_4O_{33}$ (Fig. 3a, curve 6; Fig. 3b, curve 4). Note that, despite the disappearance of the proton contribution, the total conductivity of the $La_2Nd_{12}W_4O_{33}$ and $Nd_{14}W_4O_{33}$ materials increases, reaching 7.5×10^{-5} S/cm at 600 °C in the case of the latter (Fig. 3a, curve 6). Above 700 °C, γ-$La_6W_2O_{15}$-based composite and $Nd_{14}W_4O_{33}$ differ little in conductivity in dry and wet air, which seems to be purely oxygen-ionic (Fig. 3a, curves 1 and 6). Tables 2 and 3 present activation energies for conduction in dry and wet air for samples represented in Fig. 3a and b, respectively. Even though the conductivity of $La_2Nd_{12}W_4O_{33}$ solid solution in wet air slightly exceeds that in dry air (Fig. 3a, curve 5), the contribution of proton conductivity is very small according to ac impedance measurements. The activation energies for conduction in $La_{10}W_2O_{21}$/γ-$La_6W_2O_{15}$/Ndx ($x = 0$, 2, 4, 6, 8, 10) composites in wet air between 400 and 600 °C (Tables 2 and 3) are typical of proton conductors: 0.48—0.82 eV. The activation energy of the $La_{10}W_2O_{21}$/γ-$La_6W_2O_{15}$/Ndx ($x = 0$, 2, 4, 6, 8, 10) composites in wet air is markedly lower than that in dry air. γ-$La_6W_2O_{15}$-based composite has the lowest activation energy. Total electrical conductivity of γ-$La_6W_2O_{15}$ at 11.9 kHz as a function of P_{O2} in dry atmosphere was investigated by Ivanova et al. [39]. γ-$La_6W_2O_{15}$ is mixed electronic—ionic conductor in dry atmosphere with maximum conductivity value ~1×10^{-5} S/cm at 700 °C. At $P_{O2} < 10^{-5}$ atm and T > 300 °C n-type conductivity starts to grow. Under oxidizing conditions, the electron holes also start to contribute to the total conductivity, but this effect is less pronounced. Since the γ-$La_6W_2O_{15}$-based composite consists of 80 wt% of γ-$La_6W_2O_{15}$ phase, it is not necessary to expect high values of hole conductivity under oxidizing conditions.

Fig. 3c presents the Arrhenius plots of conductivity of two-phase material with nominal composition $5La_2O_3$:$2WO_3$ including 80.6 wt% of pure $La_{10}W_2O_{21}$ phase and 19.4 wt% of γ-$La_6W_2O_{15}$ phase in dry and wet air. This composite with a high content of the fluorite-like phase $La_{10}W_2O_{21}$ (~81 wt %) (Table 1, Fig. 2 c) showed the maximum proton conductivity in wet air (1×10^{-3} at 700 °C) comparable to that of the known proton conductor $La_{6-x}WO_{12-\delta}$ ($x = 0.6$) [15,19,39].

Since electrochemical properties of pseudorhombohedral $Nd_{14}W_4O_{33}$ have not yet been studied, we measured its total conductivity as a function of oxygen partial pressure (Fig. 4a).

Table 2 – Apparent activation energy (E_a) of total conductivity temperature dependence of Nd containing γ-La$_6$W$_2$O$_{15}$-based composites (La$_{10}$W$_2$O$_{21}$/γ-La$_6$W$_2$O$_{15}$/Ndx (x = 0, 6, 8, 10)) composites and La$_{14-x}$Nd$_x$W$_4$O$_{33}$ (x = 12, 14) pseudorhombohedral solid solutions, in dry and wet air.

| Composition	Atmosphere	E_a (±0.01), eV	
		350–600 °C	600–900 °C
La$_{10}$W$_2$O$_{21}$/γ-La$_6$W$_2$O$_{15}$ (1450°C)	Dry air	0.50	1.28
	Wet air	0.48	1.09
La$_{10}$W$_2$O$_{21}$/γ-La$_6$W$_2$O$_{15}$/Nd6 (1500°C)	Dry air	0.85	1.48
	Wet air	0.68	1.35
La$_{10}$W$_2$O$_{21}$/γ-La$_6$W$_2$O$_{15}$/Nd8 (1500°C)	Dry air	0.95	1.45
	Wet air	0.76	1.34
La$_{10}$W$_2$O$_{21}$/γ-La$_6$W$_2$O$_{15}$/Nd10 (1500°C)	Dry air	1.00	1.43
	Wet air	0.82	1.37
La$_2$Nd$_{12}$W$_4$O$_{33}$ (1500°C)	Dry air	0.94	1.10
	Wet air	0.91	1.08
Nd$_{14}$W$_4$O$_{33}$ (1500°C)	Dry air	1.00	
	Wet air	0.96	

It follows from Fig. 4a that at 700 °C Nd$_{14}$W$_4$O$_{33}$ has a purely ionic conductivity of ~4 × 10^{-4} S/cm at oxygen partial pressures from 10^{-18} to 1 atm and that its 900 °C conductivity exceeds ~1 × 10^{-3} S/cm. Therefore, Nd$_{14}$W$_4$O$_{33}$ can be regarded as an oxygen ion conductor. The same conductivity (~4 × 10^{-4} S/cm at 700°C) was obtained for this sample from impedance spectroscopy data (Fig. 3b, curve 4). It is worth noting that only at 800 °C do we observe an increase in the n-type conductivity of Nd$_{14}$W$_4$O$_{33}$, which seems to be due to W^{6+} reduction at low oxygen partial pressures (P$_{O2}$ < 10^{-16} atm), and there is no hole conduction up to P$_{O2}$ ~ 1 atm. This ceramic exhibits p-type conductivity from 900 °C (P$_{O2}$ ≥ 10^{-4} atm). Thus, Nd$_{14}$W$_4$O$_{33}$ is stable under oxidizing/reducing conditions up to 700 °C. Thus, Nd$_{14}$W$_4$O$_{33}$ is a nearly pure ionic conductor up to 700 °C and mixed conductor at T ≥ 800°C.

Besides, below 600 °C the conductivity of Nd$_{14}$W$_4$O$_{33}$ in wet air slightly exceeds that in dry air. To ascertain the nature of the conductivity of Nd$_{14}$W$_4$O$_{33}$ ceramics, it was measured by the DC method in dry and wet air, wet nitrogen, and wet hydrogen (Fig. 4b). The total conductivity in wet air was found to be essentially identical to that in wet nitrogen, suggesting that there was no proton contribution [1,3]. The higher conductivity in wet hydrogen was most likely due to reduction of Nd$_{14}$W$_4$O$_{33}$ in the hydrogen atmosphere.

In the case of the low-temperature series of materials, with high neodymium content, La$_{10}$W$_2$O$_{21}$/γ-La$_6$W$_2$O$_{15}$/Nd10

Table 3 – Apparent activation energy (E_a) of total conductivity temperature dependence of γ-La$_6$W$_2$O$_{15}$-based composites (La$_{10}$W$_2$O$_{21}$/γ-La$_6$W$_2$O$_{15}$/Ndx (x = 2, 4)) and Nd$_{14}$W$_4$O$_{33}$, in dry and wet air.

Composition	Atmosphere	E_a (±0.01), eV	
		400–600 °C	600–900 °C
La$_{10}$W$_2$O$_{21}$/γ-La$_6$W$_2$O$_{15}$/Nd2 (1400°C)	Dry air	0.97	1.49
	Wet air	0.81	1.34
La$_{10}$W$_2$O$_{21}$/γ-La$_6$W$_2$O$_{15}$/Nd4 (1400°C)	Dry air	0.82	1.54
	Wet air	0.69	1.41
Nd$_{14}$W$_4$O$_{33}$ (1450°C)	Dry air	1.03	0.95
	Wet air	1.03	0.99
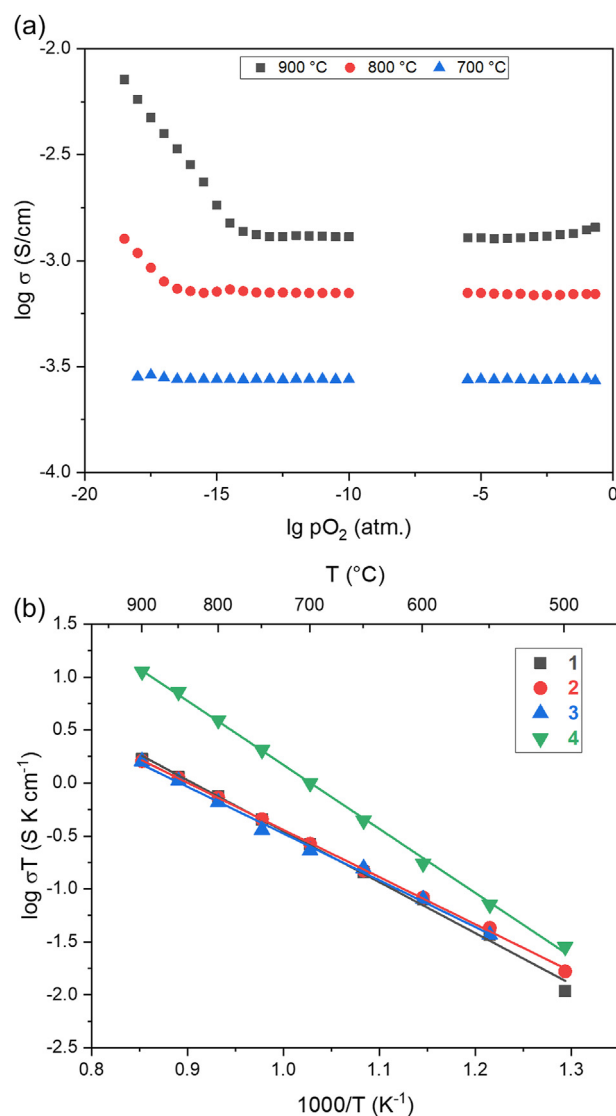
Fig. 4 – a: Total conductivity as a function of oxygen partial pressure for pseudorhombohedral Nd$_{14}$W$_4$O$_{33}$ prepared at 1450 °C. b: Total conductivity of Nd$_{14}$W$_4$O$_{33}$ prepared at 1450 °C; four-probe ac measurements in (1) dry air, (2) wet air, (3) wet nitrogen, and (4) wet hydrogen.

composite and $La_{14-x}Nd_xW_4O_{33}$ ($x = 12$, 14) solid solutions, synthesized at 1400 °C in 8 h (Fig. 5), the total conductivity of the $La_2Nd_{12}W_4O_{33}$ ($x = 2$) pseudorhombohedral solid solution is eight times higher than that of $Nd_{14}W_4O_{33}$ (Fig. 5, curves 2 and 1), and conductivity of the $La_{10}W_2O_{21}/\gamma$-$La_6W_2O_{15}/Nd10$ composite is protonic in nature (Fig. 5, curve 3).

Bespalko et al. [26] reported that the addition of lanthanum to the proton-conducting solid solution $Nd_{5.5}WO_{11.25-\delta}$ (($Nd_{5/6}La_{1/6}$)$_{5.5}WO_{11.25-\delta}$) improved its transport properties: its proton conductivity increased by an order of magnitude, to ~ 8×10^{-5} S/cm at 600 °C, and so did its oxygen ion conductivity. The proton conductivity of γ-$La_6W_2O_{15}$-based composite, consisting of ~18 wt% of $La_{10}W_2O_{21}$, is ~6×10^{-5} S/cm at 600 °C, approaching that of the Nd-rich mixed tungstate ($Nd_{5/6}La_{1/6}$)$_{5.5}WO_{11.25-\delta}$ [26]. The proton conductivity of $La_{10}W_2O_{21}$-based composite consisting of ~81 wt% of $La_{10}W_2O_{21}$ is ~7.5×10^{-4} S/cm at 600 °C, approaching that of the $La_{6-x}WO_{12-\delta}$ fluorite-like proton conductors [39]. Note that the conductivity of the pure phase $La_{10}W_2O_{21}$ is ~4×10^{-5} S/cm at 600 °C in ambient air [12], whereas for $La_{10}W_2O_{21}$-based composite, consisting of ~81 wt % of $La_{10}W_2O_{21}$, conductivity attains ~4×10^{-4} S/cm at 600 °C in dry air. We can assume a composite effect, which has recently been demonstrated for $La_2Mo_2O_9$–$La_2Mo_3O_{12}$ composite oxygen-ion electrolytes [47].

Thus, proton conductivity decreases with decreasing La_2O_3 content in the lanthanum tungstate system in the following order: $La_{6-x}WO_{12-\delta}$ ($x = 0.3$–0.7) $\geq$ composite material based on $La_{10}W_2O_{21}$ > composite material based on γ-$La_6W_2O_{15}$ > γ-$La_6W_2O_{15}$.

In the case of the pseudorhombohedral structure of $La_{14-x}Nd_xW_4O_{33}$ ($x = 12$, 14) solid solutions, proton conductivity is negligible, whereas oxygen ion conductivity rises, reaching ~ 4×10^{-4} S/cm at 700 °C for $Nd_{14}W_4O_3$ synthesized at 1450–1500 °C, which allows it to be viewed as a new oxygen ion conductor (Fig. 4a and b).

Difficulties in synthesis of lanthanum neodymium tungstates with high conductivity

It should be emphasized that the conductivity of $Nd_{14}W_4O_{33}$ is a rather strong function of synthesis conditions. Fig. 6 shows Arrhenius plots of conductivity for two samples differing in thermal history. Note that annealing at 1400 °C for 8 h reduced the total conductivity of the $Nd_{14}W_4O_{33}$ ceramics by an order of magnitude in comparison with the ceramics produced at 1500 °C (4 h) or 1450 °C (4 h). In this case, a short high temperature annealing is preferable to a longer low temperature annealing. This is probably due to volatility of tungsten oxide from its compounds during prolonged annealing. In a previous study [48], the composition of rare-earth molybdates with the nominal formula $Ln_{10}Mo_2O_{21}$ (Ln = Dy, Gd, Ho) was observed to change during prolonged (80–160 h) annealing at 1200 °C as a result of molybdenum oxide volatility. An unexpected result was obtained for the Nd-poor composite $La_{10}W_2O_{21}/\gamma$-$La_6W_2O_{15}/Nd2$ (Fig. S5). Raising the synthesis temperature from 1400 to 1500 °C at a constant annealing time led to degradation of its proton conductivity between 500 and 600 °C. This was possibly due to micromelting processes, which were observed between 1500 and 1600 °C in the lanthanum tungstates composites with low neodymium
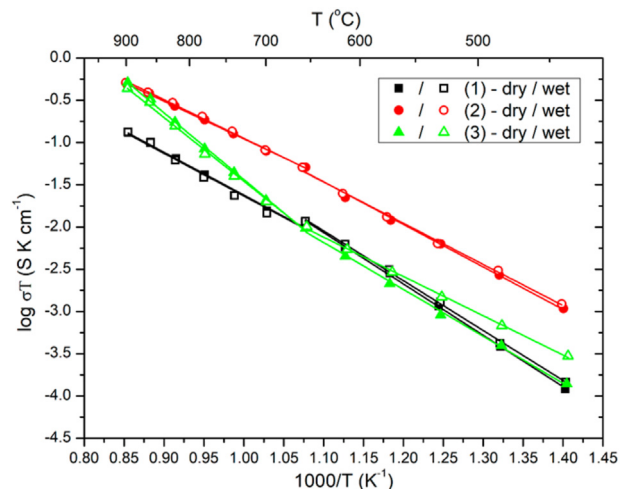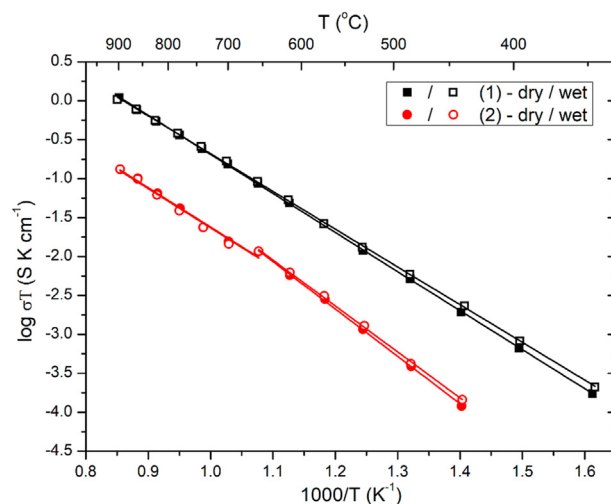
Fig. 5 – Arrhenius plots of conductivity in dry (filled data points) and wet (open data points) air for (1) pseudorhombohedral $Nd_{14}W_4O_{33}$, (2) $La_2Nd_{12}W_4O_{33}$ pseudorhombohedral solid solution, and (3) $La_{10}W_2O_{21}/\gamma$-$La_6W_2O_{15}/Nd10$ composite synthesized at 1400 °C (8 h).

content. As a rule, the melting point of rare-earth compounds decreases with increasing Ln ionic radius.

Microstructure and density of ceramics under study

Table S1 and Fig. 7 present geometric density data obtained by measurements of mass and dimensions for two series of ceramics synthesized at 1500 and 1400 °C (Fig. 7 curves 1 and 2, respectively).

In both series the density of materials shows a similar behavior, however it should be noted that sintering at 1400 °C results in a higher density than sintering at 1500 °C.

Fig. 6 – Arrhenius plots of conductivity in dry (filled data points) and wet (open data points) air for $Nd_{14}W_4O_{33}$ ceramics prepared at (1) 1500 °C (4 h) and (2) 1400 °C (8 h).
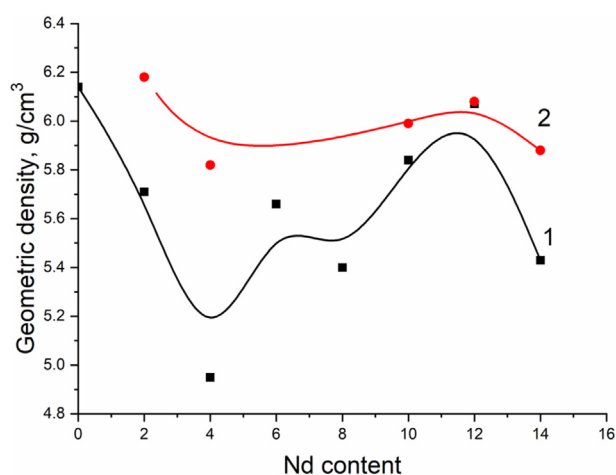
Fig. 7 – Geometric density as a function of Nd content for the $La_{10}W_2O_{21}/\gamma$-$La_6W_2O_{15}$/Ndx ($x = 0, 2, 4, 6, 8, 10, 12, 14$) ceramics prepared at (1) 1500 and (2) 1400 °C.

In the 1400 °C series, the highest density was offered by the Nd-poor $La_{10}W_2O_{21}/\gamma$-$La_6W_2O_{15}$/Nd2 composite, the Nd-rich $La_{10}W_2O_{21}/\gamma$-$La_6W_2O_{15}$/Nd10 composite, and the $La_{14-x}Nd_xW_4O_{33}$ ($x = 12$) solid solution with a pseudorhombohedral structure, also Nd-rich. In addition, $La_{14-x}Nd_xW_4O_{33}$ ($x = 12$) solid solution had the highest oxygen ion conductivity.

The appearance of the ceramics is given in Table S1. It is worth noting the change in color from yellow to purple with increasing Nd content and the surface roughness of the pellets, which was found to increase with La content and also with temperature in the case of $La_{10}W_2O_{21}/\gamma$-$La_6W_2O_{15}$ composite material. We assume that this was due to micromelting on the ceramic surface. The best Ln/W ratios near to the formula composition (Ln/W = 3.5) were obtained for $La_{10}W_2O_{21}/\gamma$-$La_6W_2O_{15}$/Ndx ($x = 2, 4, 10$) composites (Table 4). For γ-$La_6W_2O_{15}$-based composite material and $Nd_{14}W_4O_{33}$, there is some excess of lanthanum or neodymium, respectively. It should be noted the uniform distribution of Ln (Ln = La, Nd) cations in all the studied samples, which confirms the assumption that neodymium is uniformly incorporated into the sublattice of fluorite-like $La_{10}W_2O_{21}$ ($5La_2O_3$:$2WO_3$) and

orthorhombic γ-$La_6W_2O_{15}$ ($3La_2O_3$:$2WO_3$) tungstates (Fig. S6a-d). The microstructure of the polished and thermal etched ceramic surface for the samples under discussion is shown in Fig. 8. Comparing the SEM images of the polished and thermally etched surfaces, it should be noted that the least porous ceramics were the Nd-poor $La_{10}W_2O_{21}/\gamma$-$La_6W_2O_{15}$/Nd2 composite, the Nd-rich $La_{10}W_2O_{21}/\gamma$-$La_6W_2O_{15}$/Nd10 composite, and the $La_{14-x}Nd_xW_4O_{33}$ ($x = 12$) solid solution (Fig. 8b, d, e). The γ-$La_6W_2O_{15}$-based composite material (Fig. 8a) had lower porosity than that of the single phase $Nd_{14}W_4O_{33}$ (Fig. 8f). The results obtained are consistent with the density data shown in Fig. 7, curve 2.

The unusual surface morphology of γ-$La_6W_2O_{15}$-based composite should be noted (Fig. 8a). On the polished and thermally etched surface of this sample, the cracks can be seen passing mainly along the grain boundaries (Fig. 8a. The arrows mark the cracks). This may indicate the influence of a reversible phase transition in this composite ceramic, which will be discussed in the next paragraph. Previously Ivanova et al. [39] had already observed a high crack density in as-sintered γ-$La_6W_2O_{15}$ ceramics ($T_{syn.} = 1400$ °C), that were associated with polymorphism phenomena, typical of the orthorhombic phase. A similar behavior was observed in related lanthanum tungstates $Ln_2W_2O_9$ (Ln_2O_3:$2WO_3$) (Ln = Ce, Nd, Pr, Sm, Eu, Gd and Tb) due to a significant volume change during low-temperature phase transformation [49]. A linear relationship between the phase transition temperature and the ionic radii of the rare-earth cation was found, ranging from 325 °C for $Pr_2W_2O_9$ to 600 °C for $Gd_2W_2O_9$. For the rest of the composite and solid solution ceramics, synthesized at 1400 °C in this study, this phenomenon of cracking was not observed (Fig. 8b–f).

Next, the second series of ceramics synthesized at 1500°C was studied. In this case, cracks are present in the $La_{10}W_2O_{21}/\gamma$-$La_6W_2O_{15}$/Ndx ($x = 2, 4, 6, 8$) γ-$La_6W_2O_{15}$-based composites and can be attributed to the evaporation of WO_3 from the composites at temperatures ~ 1500 °C (Fig. S7b-e). EDX data supported this conclusion (Fig. S6e, f). Lanthanum and neodymium are uniformly incorporated into the sublattice of the fluorite-like $La_{10}W_2O_{21}$ and orthorhombic γ- $La_6W_2O_{15}$ composite phases, but there is a lack of tungsten, mainly in the pore regions (Fig. S6e, f). More neodymium should to be added to the composite to suppress cracking at 1500 °C synthesis

Table 4 – SEM/EDX point analysis data of polished and thermal etched surfaces of Nd containing γ-$La_6W_2O_{15}$-based composites ($La_{10}W_2O_{21}/\gamma$-$La_6W_2O_{15}$/Ndx ($x = 0, 2, 4, 6, 8, 10$)) and $La_{14-x}Nd_xW_4O_{33}$ ($x = 12, 14$) solid solutions under investigation.

Composition	(La + Nd)/W ratio (formula)	(La + Nd)/W ratio (averaging over 5 spectra) $T_{syn.} = 1400$ °C, 4–8 h	(La + Nd)/W ratio (averaging over 5 spectra) $T_{syn.} = 1500$ °C, 2–4 h	Analysis area (μm^2)
$La_{10}W_2O_{21}/\gamma$-$La_6W_2O_{15}$	3.50	3.91 ± 0.05[a]	–	140×200
$La_{10}W_2O_{21}/\gamma$-$La_6W_2O_{15}$/Nd2		3.84 ± 0.07	3.85 ± 0.04	
$La_{10}W_2O_{21}/\gamma$-$La_6W_2O_{15}$/Nd4		3.79 ± 0.06	3.84 ± 0.04	
$La_{10}W_2O_{21}/\gamma$-$La_6W_2O_{15}$/Nd6		–	4.72 ± 0.2	
$La_{10}W_2O_{21}/\gamma$-$La_6W_2O_{15}$/Nd8		–	4.09 ± 0.05	
$La_{10}W_2O_{21}/\gamma$-$La_6W_2O_{15}$/Nd10		3.76 ± 0.08	3.78 ± 0.17	
$La_{14-x}Nd_xW_4O_{33}$ ($x = 12$)		4.04 ± 0.1	4.12 ± 0.08	
$Nd_{14}W_4O_{33}$		4.03 ± 0.03	3.94 ± 0.07	

[a] For $La_{10}W_2O_{21}/\gamma$-$La_6W_2O_{15}$ composite $T_{syn.} = 1450$ °C, 4 h.
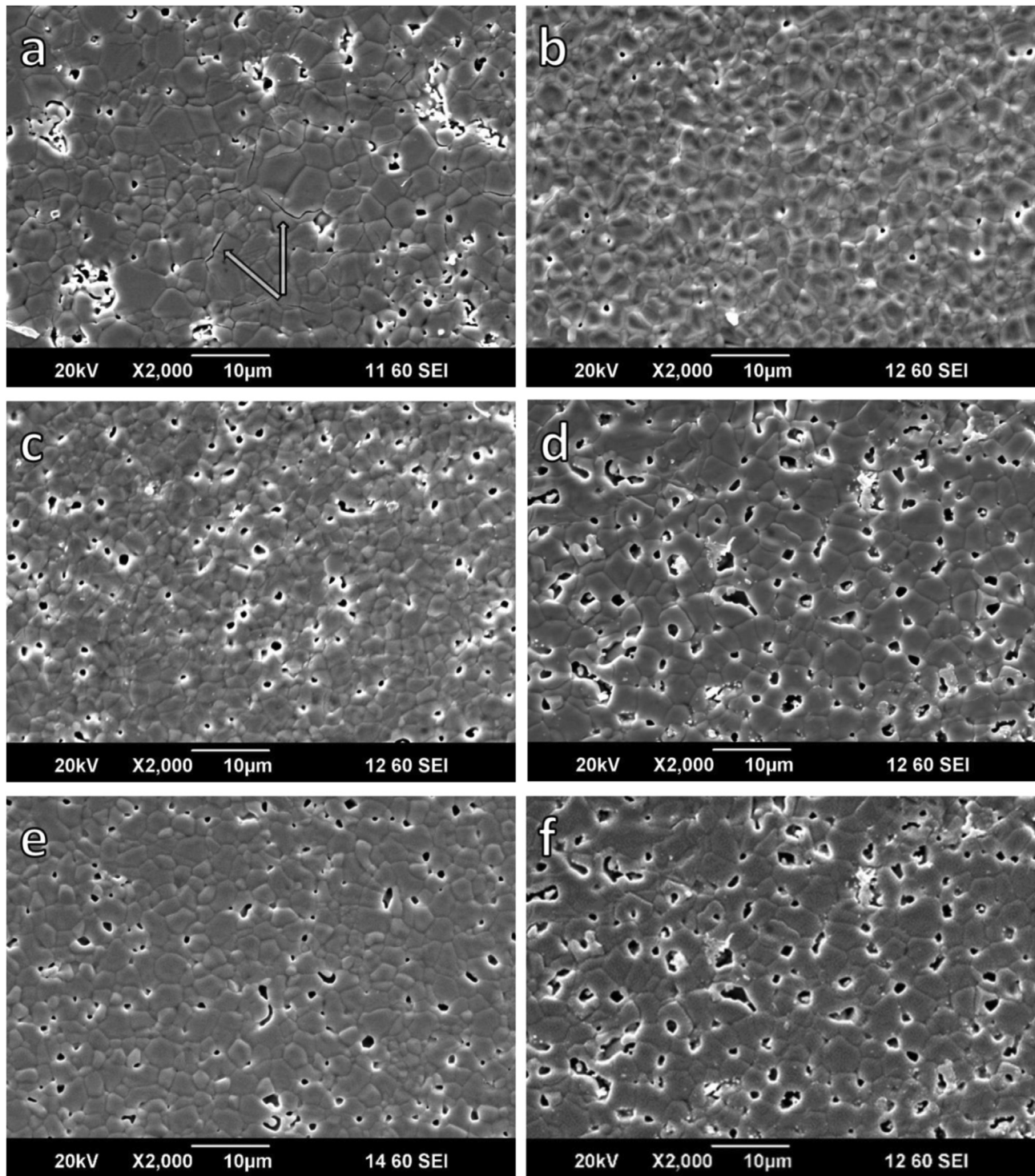
Fig. 8 — SEM images of polished and thermal etched surfaces of (a) $La_{10}W_2O_{21}/\gamma$-$La_6W_2O_{15}$ composite, (b) $La_{10}W_2O_{21}/\gamma$-$La_6W_2O_{15}/Nd2$ composite, (c) $La_{10}W_2O_{21}/\gamma$-$La_6W_2O_{15}/Nd4$ composite, (d) $Nd_{14}W_4O_{33}$, synthesized in the 1400—1450 °C temperature interval; and (e) $La_{10}W_2O_{21}/\gamma$-$La_6W_2O_{15}/Nd2$ composite, (f) $La_{10}W_2O_{21}/\gamma$-$La_6W_2O_{15}/Nd4$ composite, (g) $Nd_{14}W_4O_{33}$ synthesized at 1500 °C. The arrows mark cracks.

temperatures. No cracking was observed in the $La_{10}W_2O_{21}/\gamma$-$La_6W_2O_{15}/Ndx$ ($x = 10$) composite and pseudorhombohedral $La_{14-x}Nd_xW_4O_{33}$ ($x = 12, 14$) ceramics (Fig. S7f, g, h). However, a lack of tungsten was also observed in these Nd-rich samples (Fig. S6 g).

Thus, annealing at a higher temperature of 1500°C reduces the density of Nd-containing composites due to the evaporation of WO_3, which leads to a decrease in the density of the samples, as shown in Fig. 7, curve 1. No cracking was observed in the $La_{10}W_2O_{21}/\gamma$-$La_6W_2O_{15}/Ndx$ ($x = 10$) Nd-rich composite.

Under a temperature annealing at 1400°C, there were no cracks for Nd-containing γ-La$_6$W$_2$O$_{15}$-based composite ceramics. For γ-La$_6$W$_2$O$_{15}$-based composites, formation of cracks associated with the polymorphism of the γ-La$_6$W$_2$O$_{15}$ phase was found after 1450°C temperature annealing. No cracking was observed in the pseudorhombohedral La$_{14-x}$Nd$_x$W$_4$O$_{33}$ (x = 12, 14) ceramics, synthesized at 1400 and 1500°C.

Effect of Nd addition on the phase transition of γ-La$_6$W$_2$O$_{15}$-based composite material

In this work, reversible phase transitions known for γ-La$_6$W$_2$O$_{15}$ [37,39] were studied for γ-La$_6$W$_2$O$_{15}$-based composite, Nd$_{14}$W$_4$O$_{33}$, and La$_{10}$W$_2$O$_{21}$/γ-La$_6$W$_2$O$_{15}$/Ndx (x = 2, 4, 6, 8, 10) composite powders by DSC in the range of 25–1000 °C. Since the γ-La$_6$W$_2$O$_{15}$ composite is a two-phase material consisting not only of γ-La$_6$W$_2$O$_{15}$ (3La$_2$O$_3$:2WO$_3$) but also of the fluorite-related cubic phase La$_{10}$W$_2$O$_{21}$ (5La$_2$O$_3$:2WO$_3$), it was important to understand how the presence of two phases influences the phase transitions typical for γ-La$_6$W$_2$O$_{15}$ (3La$_2$O$_3$:2WO$_3$). During heating of γ-La$_6$W$_2$O$_{15}$-based composite in a DSC cell, only one endothermic peak was detected at 910 °C, whereas in the case of γ-La$_6$W$_2$O$_{15}$ Chambrier et al. [37]. observed two endothermic peaks, at 615 and 944 °C, which corresponded to reversible phase transitions. One of them was due to the transition from the low-temperature (γ) phase to the intermediate-temperature (β) phase, and the other was due to the transition from the β phase to the high-temperature (α) phase [37]. Reversible phase transitions below 900 °C are undesirable in candidate materials for use in hydrogen generation membranes and solid oxide fuel cells. Thus, it is seen that unlike γ-La$_6$W$_2$O$_{15}$, the γ-La$_6$W$_2$O$_{15}$-based composite undergoes no phase transition at 615 °C, and its DSC curves show only one reversible transition at 910 °C (Fig. 9).

For 1400 °C series, an introduction of a small amount of Nd in the γ-La$_6$W$_2$O$_{15}$-based composite (La$_{10}$W$_2$O$_{21}$/γ-La$_6$W$_2$O$_{15}$/Nd2) causes the 910 °C transition to disappear (Fig. S8a). Nd$_{14}$W$_4$O$_{33}$ also undergoes no transition at 910 °C (Fig. S8b). Obviously, the reversible phase transition found for the γ-La$_6$W$_2$O$_{15}$-based composite affects the microstructure of the sample. We observed the cracking phenomenon only for the γ-La$_6$W$_2$O$_{15}$-based composite (Fig. 8a), which is characterized by the reversible phase transition. For the rest of the Nd-containing ceramics synthesized at 1400 °C, this phenomenon was not observed (Fig. 8 b-g). However, synthesis at a higher temperature of 1500°C led to the evaporation of WO$_3$ even from Nd containing composites (La$_{10}$W$_2$O$_{21}$/γ-La$_6$W$_2$O$_{15}$/Ndx (x = 2, 4)) and formation of cracks (Fig. S7 b,c). At the same time, the density of ceramics decreased. Nd$_{14}$W$_4$O$_{33}$ - based solid solution ceramics do not tend to crack (Fig. S7 g, h).

Conclusions

The present results demonstrate that 7La$_2$O$_3$:4WO$_3$ composition is a two-phase material (composite) consisting of the fluorite-related La$_{10}$W$_2$O$_{21}$ (5La$_2$O$_3$:2WO$_3$) phase and the orthorhombic γ-La$_6$W$_2$O$_{15}$ (3La$_2$O$_3$:2WO$_3$) phase, whereas Nd$_{14}$W$_4$O$_{33}$ is a compound, whose structure has pseudorhombohedral cell. We have investigated structural transformations in a series of
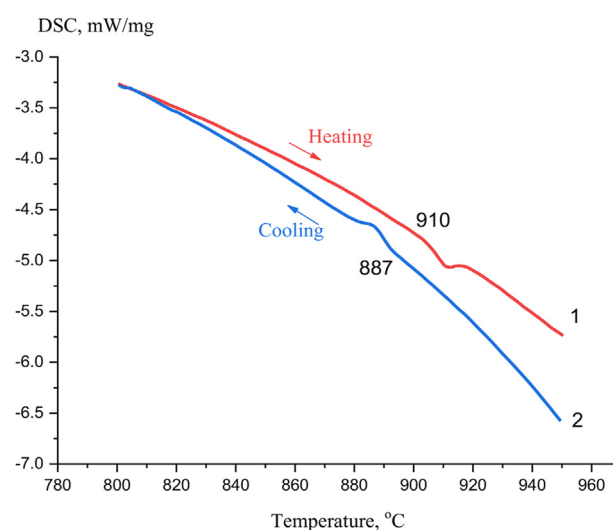
Fig. 9 – DSC data obtained during heating and cooling of the γ-La$_6$W$_2$O$_{15}$-based composite (La$_{10}$W$_2$O$_{21}$/γ-La$_6$W$_2$O$_{15}$), which demonstrate a reversible phase transition at ~ 910 °C (heating).

materials with the nominal composition La$_{14-x}$Nd$_x$W$_4$O$_{33}$ (x = 0, 2, 4, 6, 8, 10, 12, 14) and showed that La$_{14-x}$Nd$_x$W$_4$O$_{33}$ (x = 2, 4, 6, 8, 10) materials are also two-phase ones, i.e., La$_{10}$W$_2$O$_{21}$/γ-La$_6$W$_2$O$_{15}$/Ndx (x = 2, 4, 6, 8, 10). According to EDX data neodymium is uniformly incorporated into the sublattice of fluorite-like La$_{10}$W$_2$O$_{21}$ (5La$_2$O$_3$:2WO$_3$) and orthorhombic γ-La$_6$W$_2$O$_{15}$ (3La$_2$O$_3$:2WO$_3$) tungstates.

The Nd-rich La$_{14-x}$Nd$_x$W$_4$O$_{33}$ (x = 12, 14) solid solutions have a pseudorhombohedral structure. During heating in a DSC cell, the γ-La$_6$W$_2$O$_{15}$-based composite was observed to undergo a single reversible phase transition at 910 °C, whereas Nd introduction in the γ-La$_6$W$_2$O$_{15}$-based composite materials (La$_{10}$W$_2$O$_{21}$/γ-La$_6$W$_2$O$_{15}$/Ndx (x = 2, 6, 8, 10, 12, 14)) suppresses the transition.

The oxygen ion and proton conductivity of the mixed lanthanum neodymium tungstates has been studied using impedance spectroscopy, and their proton conductivity has been shown to decrease gradually with increasing Nd content. Clearly, the proton conductivity of γ-La$_6$W$_2$O$_{15}$-based composite is contributed by proton transport in both of its constituent phases: La$_{10}$W$_2$O$_{21}$ (5La$_2$O$_3$:2WO$_3$) and γ-La$_6$W$_2$O$_{15}$ (3La$_2$O$_3$:2WO$_3$). However, the proton contribution of La$_{10}$W$_2$O$_{21}$/γ-La$_6$W$_2$O$_{15}$ is mainly dependent on the proton contribution of La$_{10}$W$_2$O$_{21}$, because the proton conductivity of γ-La$_6$W$_2$O$_{15}$ is an order of magnitude lower than that of the γ-La$_6$W$_2$O$_{15}$-based composite. This point was confirmed in the present work by proton conductivity measurements of the La$_{10}$W$_2$O$_{21}$-based composite with a high content of the fluorite-like cubic phase (~81 wt% La$_{10}$W$_2$O$_{21}$). The proton conductivity of La$_{10}$W$_2$O$_{21}$-based composite is ~7.5 × 10^{-4} S/cm at 600 °C, approaching that of La$_{6-x}$WO$_{12-\delta}$ proton conductors.

At the same time, no proton conductivity has been detected in the pseudorhombohedral solid solution La$_{14-x}$Nd$_x$W$_4$O$_{33}$ (x = 12) or Nd$_{14}$W$_4$O$_{33}$, whereas their oxygen ion conductivity has been shown to rise. This behavior is due to the change in

the structure type. $Nd_{14}W_4O_{33}$ has been shown to have a wide range of ionic conductivity, which is ~4×10^{-4} S/cm at 700 °C (1.0×10^{-3} S/cm at 900 °C). This allows this compound to be viewed as a new oxygen ion conductor. Oxygen ion conduction in $Nd_{14}W_4O_{33}$ has been confirmed by four-probe ac measurements in different dry and wet gaseous atmospheres (air, nitrogen, and hydrogen). The cracking process disappears in γ-$La_6W_2O_{15}$-based composites with increasing Nd content. More neodymium should to be added to the composite to suppress cracking at higher synthesis temperatures.

Credit authorship contribution statement

A.V. Shlyakhtina: Conceptualization; Methodology; Writing - Original Draft, Review & Editing. **E.D. Baldin:** Investigation; Formal analysis; Writing - Review & Editing. **G.A. Vorobieva:** Investigation; Formal analysis. **I.V. Kolbanev:** Investigation; Resources. **D.N. Stolbov:** Investigation; Formal analysis; Visualization. **A.V. Kasyanova:** Investigation; Formal analysis, Writing - Review & Editing. **N.V. Lyskov**: Investigation; Formal analysis.

Declaration of competing interest

The authors declare that they have no known competing financial interests or personal relationships that could have appeared to influence the work reported in this paper.

Acknowledgement

Appendix A. Supplementary data

Supplementary data to this article can be found online at https://doi.org/10.1016/j.ijhydene.2023.03.259.

REFERENCES

[1] Shlyakhtina AV, Lyskov NV, Nikiforova GE, Kasyanova AV, Vorobieva GA, Kolbanev IV, et al. Proton conductivity of La$_2$(Hf$_{2-x}$La$_x$)O$_{7-x/2}$ "stuffed" pyrochlores. Appl Sci 2022;12:4342. https://doi.org/10.3390/app12094342.

[2] Dunyushkina LA. Solid oxide fuel cells with a thin film electrolyte: a review on manufacturing technologies and electrochemical characteristics. EM&T 2022;1:20221006. https://doi.org/10.15826/elmattech.2022.1.006.

[3] Kasyanova AV, Rudenko AO, Lyagaeva YuG, Medvedev DA. Lanthanum-containing proton-conducting electrolytes with perovskite structures. Membr Membr Technol 2021;3:73–97. https://doi.org/10.1134/S2517751621020050.

[4] Filonova E, Medvedev D. Recent progress in the design, characterisation and application of LaAlO$_3$- and LaGaO$_3$-based solid oxide fuel cell electrolytes. Nanomaterials 2022;12. https://doi.org/10.3390/nano12121991.

[5] Kravchyk KV, Quarez E, Solís C, Serra JM, Joubert O. Cathode materials for La$_{0.995}$Ca$_{0.005}$NbO$_4$ proton ceramic electrolyte. Int J Hydrogen Energy 2011;36:13059–66. https://doi:10.1016/j.ijhydene.2011.07.069.

[6] Lacorre P, Goutenoire F, Bohnke O, Retoux R, Laligant Y. Designing fast oxide-ion conductors based on La$_2$Mo$_2$O$_9$. Nature 2000;404:856–8. https://doi.org/10.1038/35009069.

[7] Pautonnier A, Coste S, Barre M, Lacorre Ph. Higher lanthanum molybdates: structure, crystal chemistry and properties. Prog Solid State Chem 2022. https://doi.org/10.1016/j.progsolidstchem.2022.100382. Available online 17 November 2022.

[8] López-Vergara A, Porras-Vázquez JM, Infantes-Molina A, Canales-Vázquez J, Cabeza A, Losilla ER, Marrero-López D. Effect of preparation conditions on the polymorphism and transport properties of La$_{6-x}$MoO$_{12-\delta}$ ($0 \leq x \leq 0.8$). Chem Mater 2017;29:6966–75. https://doi.org/10.1021/acs.chemmater.7b02481.

[9] Shlyakhtina AV, Lyskov NV, Kolbanev IV, Shchegolikhin AN, Karyagina OK, Shcherbakova LG. Key trends in the proton conductivity of Ln$_{6-x}$MoO$_{12-\delta}$ (Ln = La, Nd, Sm, Gd -Yb; $x = 0$, 0.5, 0.6, 0.7, 1) rare-earth molybdates. Int J Hydrogen Energy 2021;46:16989–98. https://doi.org/10.1016/j.ijhydene.2021.01.129.

[10] Shlyakhtina AV, Savvin SN, Lyskov NV, Kolbanev IV, Karyagina OK, Chernyak SA, Shcherbakova LG, Núñez P. Polymorphism in the family of Ln$_{6-x}$MoO$_{12-\delta}$ (Ln = La, Gd–Lu; $x = 0$, 0.5) oxygen ion- and proton-conducting materials. J Mater Chem 2017;5:7618–30. https://doi.org/10.1039/C6TA09963G.

[11] Marrero-López D, Peña-Martínez J, Ruiz-Morales JC, Núñez P. Phase stability and ionic conductivity in substituted La$_2$W$_2$O$_9$. J Solid State Chem 2008;181:253–62. https://doi.org/10.1016/j.jssc.2007.11.024.

[12] Chambrier M-H, Le Bail A, Giovannelli F, Redjaïmia A, Florian P, Massiot D, Suard E, Goutenoire F. La$_{10}$W$_2$O$_{21}$: an anion-deficient fluorite-related superstructure with oxide ion conduction. Inorg Chem 2014;53:147–59. https://doi.org/10.1021/ic401801u.

[13] Shimura T, Fujimoto S, Iwahara H. Proton conduction in non-perovskite-type oxides at elevated temperatures. Solid State Ionics 2001;143:117–23. https://doi.org/10.1016/S0167-2738(01)00839-6.

[14] Magrasó A, Frontera C, Marrero-López D, Núñez P. New crystal structure and characterization of lanthanum tungstate "La$_6$WO$_{12}$" prepared by freeze-drying synthesis. Dalton Trans 2009:10273. https://doi.org/10.1039/b916981b.

[15] Magrasó A, Haugsrud R. Effects of the La/W ratio and doping on the structure, defect structure, stability and functional properties of proton-conducting lanthanum tungstate La$_{28-x}$W$_{4+x}$O$_{54+\delta}$. A review. J Mater Chem 2014;2:12630–41. https://doi.org/10.1039/C4TA00546E.

[16] Erdal S, Kalland L-E, Hanske R, Polfus J, Haugsrud R, Norby T, Magrasó A. Defect structure and its nomenclature for mixed

conducting lanthanum tungstates $La_{28-x}W_{4+x}O_{54+3x/2}$. Int J Hydrogen Energy 2012;37:8051–5.

[17] Zhu S, Drazkowski M, Boukamp BA, Bouwmeester HJM. On the effect of electrode material in electrical conductivity relaxation - an alternative interpretation of the two-fold relaxation behavior in $La_{5.4}WO_{11.1-\delta}$. Solid State Ionics 2022;384:115994. https://doi.org/10.1016/j.ssi.2022.115994.

[18] Escolastico S, Seeger J, Roitsch S, Ivanova M, Meulenberg WA, Serra JM. Enhanced H_2 separation through mixed proton-electron conducting membranes based on $La_{5.5}W_{0.8}M_{0.2}O_{11.25-\delta}$. ChemSusChem 2013;6:1523–32. https://doi.org/10.1002/cssc.201300091.

[19] Magrasó A. Transport number measurements and fuel cell testing of undoped and Mo-substituted lanthanum tungstate. J Power Sources 2013;240:583–8. https://doi.org/10.1016/j.jpowsour.2013.04.087.

[20] Polfus JM, Li Z, Xing W, Sunding MF, Walmsley JC, Fontaine M-L, Henriksen PP, Bredesen R. Chemical stability and H_2 flux degradation of cercer membranes based on lanthanum tungstate and lanthanum chromite. J Membr Sci 2016;503:42–7. https://doi.org/10.1016/j.memsci.2015.12.054.

[21] Pestereva N, Guseva A, Vyatkin I, Lopatin D. Electrotransport in tungstates $Ln_2(WO_4)_3$ (Ln = La, Sm, Eu, Gd). Solid State Ionics 2017;301:72–7. https://doi.org/10.1016/j.ssi.2017.01.009.

[22] Pestereva NN, Lopatin DA, Guseva AF, Vostrotina EL, Korona DV, Nokhrin SS. Electric transport in tungstates $Ln_2(WO_4)_3$ (Ln = Yb, Lu). Russ J Electrochem 2017;53:744–51. https://doi.org/10.1134/S1023193517070084.

[23] Escolástico S, Stournari V, Malzbender J, Haas-Santo K, Dittmeyer R, Serra JM. Chemical stability in H_2S and creep characterization of the mixed protonic conductor $Nd_{5.5}WO_{11.25-\delta}$. Int J Hydrogen Energy 2018;43:8342–54. https://doi.org/10.1016/j.ijhydene.2018.03.060.

[24] Escolástico S, Solís C, Haugsrud R, Magrasó A, Serra JM. On the ionic character of H_2 separation through mixed conducting $Nd_{5.5}W_{0.5}Mo_{0.5}O_{11.25-\delta}$ membrane. Int J Hydrogen Energy 2017;42:11392–9. https://doi.org/10.1016/j.ijhydene.2017.02.087.

[25] Escolástico S, Solís C, Serra JM. Study of hydrogen permeation in $(La_{5/6}Nd_{1/6})_{5.5}WO_{12-\delta}$ membranes. Solid State Ionics 2012;216:31–5. https://doi.org/10.1016/j.ssi.2011.11.004.

[26] Bespalko Y, Eremeev N, Skryabin P, Krieger T, Chesalov Y, Lapina O, Khabibulin D, Ulihin A, Uvarov N, Sadykov V. Structural and transport properties of neodymium tungstates prepared via mechanochemical activation. Ceram Int 2019;45:9529–36. https://doi.org/10.1016/j.ceramint.2018.09.277.

[27] Ding J, Balachandran J, Sang X, Guo W, Anchell JS, Veith GM, Bridges CA, Cheng Y, Rouleau CM, Poplawsky JD, Bassiri-Gharb N, Unocic RR, Ganesh P. The influence of local distortions on proton mobility in acceptor doped perovskites. Chem Mater 2018;30:4919–25. https://doi.org/10.1021/acs.chemmater.8b00502.

[28] McCarthy GJ, Fischer RD, Jonson GG, Gooden CE. Crystal chemistry and compound formation in the systems rare earth sesquioxide-WO_3. J Solid State Chem 1972;364:397–410.

[29] Chang LLY, Scroger MG, Phillips B. High temperature phase equilibria in the systems Sm_2O_3-WO_3 and Sm_2O_3-W-WO_3. J Inorg Nucl Chem 1966;28:1179–84. https://doi.org/10.1016/0022-1902(66)80443-8.

[30] McCarthy GJ, Fischer RD, Sanzgiri J. Crystal chemistry and subsolidus phase relations in the system Eu-W-O. J Solid State Chem 1972;5:200–6. https://doi.org/10.1016/0022-4596(72)90029-1.

[31] McCarthy GJ, Fischer RD. Synthesis and x-ray study of fluorite related phases in the system Ho_2O_3-WO_3. Mater Res Bull 1971;6:591–602. https://doi.org/10.1016/0025-5408(71)90008-0.

[32] Nilsson M, Grins J, Käll P-O, Svensson G. Synthesis, structural characterisation and magnetic properties of $Gd_{14}W_4O_{33-x}N_y$ ($0 \leqslant x \leqslant 17 \pm 2$, $0 \leqslant y \leqslant 9 \pm 2$), a new fluorite-related oxynitride. J Alloys Compd 1996;240:60–9. https://doi.org/10.1016/0925-8388(96)02325-0.

[33] Yoshimura M, Rouanet A. High temperature phase relation in the system La_2O_3-WO_3. Mater Res Bull 1976;11:151–8. https://doi.org/10.1016/0025-5408(76)90070-2.

[34] Yoshimura M, Sibieude F, Rouanet A, Foex M. Identication of binary compounds in the system Ce_2O_3-WO_3 n.d.:14.

[35] Rode EYa, Karpov VN. Phase diagram of the system Nd_2O_3-WO_3. Izv Acad Nauk SSSR, Neorgan Mater 1968;2:683.

[36] Chambrier M-H. Analyse structurale au sein du diagramme de phase de La_2O_3-WO_3 et exploration des propriétés de conduction ionique. Extended Abstract of Doct. Sci. (Chem.). Maine; 2009.

[37] Chambrier M-H, Ibberson RM, Goutenoire F. Structure determination of α-$La_6W_2O_{15}$. J Solid State Chem 2010;183:1297–302. https://doi.org/10.1016/j.jssc.2010.03.043.

[38] Yoshimura M. X-ray characterization and thermal properties of $3R_2O_3 2WO_3$ compounds (R = La, Ce, Pr, and Nd). J Am Ceram Soc 1977;60:77–8. https://doi.org/10.1111/j.1151-2916.1977.tb16100.x.

[39] Ivanova ME, Seeger J, Serra JM, Solis C, Meulenberg WA, Roitsch S, Buchkremer HP. Influence of the $La_6W_2O_{15}$ phase on the properties and integrity of $La_{6-x}WO_{12-\delta}$–based membranes. Chem Mater Res 2012;2:27–81.

[40] Shlyakhtina A, Lyskov N, Cheryak S, Kolbanev I, Kasyanova A, Medvedev D. Oxygen-ion conductivity of Re tungstates $Ln_{14}W_4O_{33}$ (Ln = Nd, Sm, Gd). In: IEEE international symposium on applications of ferroelectrics. ISAF; 2021. p. 1–2. https://doi.org/10.1109/ISAF51943.2021.9477315. 2021.

[41] Aronov MN. Laboratory vibrating eccentric mill. 1959.

[42] Aronov MN, Morgulis LM. 113794, [n.d.].

[43] Kolbanev IV, Shlyakhtina AV, Degtyarev EN, Eyu K, Lyskov NV, Stolbov DN, et al. Room-temperature mechanochemical synthesis of RE molybdates: Impact of structural similarity and basicity of oxides. J Am Ceram Soc 2021;104:5698–710. https://doi.org/10.1111/jace.17939.

[44] Hill RJ, Howard CJ. Quantitative phase analysis from neutron powder diffraction data using the Rietveld method. J Appl Crystallogr 1987;20:467–74. https://doi.org/10.1107/S0021889887086199.

[45] Shlyakhtina AV, Lyskov NV, Avdeev M, Goffman VG, Gorshkov NV, Knotko AV, Kolbanev IV, Karyagina OK, Maslakov KI, Shcherbakova LG, Sadovskaya EM, Sadykov VA, Eremeev NF. Comparative study of electrical conduction and oxygen diffusion in the rhombohedral and bixbyite Ln_6MoO_{12} (Ln = Er, Tm, Yb) polymorphs. Inorg Chem 2019;58:4275–88. https://doi.org/10.1021/acs.inorgchem.8b03397.

[46] López-Vergara A, Vizcaíno-Anaya L, Porras-Vázquez JM, Baldinozzi G, Santos-Gómez L dos, Canales-Vazquez J, Marrero-López D, Losilla ER. Unravelling crystal superstructures and transformations in the $La_{6-x}MoO_{12-\delta}$ ($0.6 \leq x \leq 3.0$) series: a system with tailored ionic/electronic conductivity. Chem Mater 2020;32:7052–62. https://doi.org/10.1021/acs.chemmater.0c02673.

[47] Porotnikova N, Khrustov A, Farlenkov A, Khodimchuk A, Partin G, Animitsa I, KochetovaPavlovAnanyev N, Kochetova D, Pavlov M, Ananyev. Promising $La_2Mo_2O_9$–$La_2Mo_3O_{12}$ composite oxygen-ionic electrolytes: interphase phenomena. ACS Appl Mater Interfaces 2022;14(4):6180–93. https://doi.org/10.1021/acsami.1c20839.

[48] Shlyakhtina AV, Avdeev M, Lyskov NV, Abrantes JCC, Gomes E, Denisova KN, Kolbanev IV, Chernyak SA,

Volkova OS, Vasiliev AN. Structure, conductivity and magnetism of orthorhombic and fluorite polymorphs in $MoO_3-Ln_2O_3$ (Ln = Gd, Dy, Ho) systems. Dalton Trans 2020;49:2833−42. https://doi.org/10.1039/C9DT04724G.

[49] Marrero-López D, Canales-Vázquez J, Ruiz-Morales JC, Núñez P. High temperature properties of rare-earth tungstates $RE_2W_2O_9$. J Alloys Compd 2015;622:557−64. https://doi.org/10.1016/j.jallcom.2014.10.139.